

# Low-threshold, cw, all-solid-state Ti:Al<sub>2</sub>O<sub>3</sub> laser

James Harrison, Andrew Finch, David M. Rines, Glen A. Rines, and Peter F. Moulton

Schwartz Electro-Optics, Inc., Research Division, 45 Winthrop Street, Concord, Massachusetts 01742

Received November 27, 1990; accepted February 15, 1991

A cw Ti:Al<sub>2</sub>O<sub>3</sub> ring laser with a threshold power of 119 mW is demonstrated. It provides a tunable source of single-frequency, diffraction-limited radiation that is suitable for injection seeding. The Ti:Al<sub>2</sub>O<sub>3</sub> laser is operated with a diode-laser-pumped, frequency-doubled, Nd:YAG laser as the sole pump source.

Titanium-doped sapphire (Ti:Al<sub>2</sub>O<sub>3</sub>) has emerged as an important laser medium owing to its broad coverage of the near-infrared spectral region (~0.7–1.1 μm). Improvements in crystal preparation have led to rapid commercialization of both cw and pulsed Ti:Al<sub>2</sub>O<sub>3</sub> lasers. These are longitudinally pumped, typically by Ar-ion or lamp-pumped, frequency-doubled, Nd lasers. The prospect of employing diode-laser-pumped versions of the latter laser is of great interest for applications such as space-based remote sensing that emphasize efficiency, lifetime, and structural integrity. The first all-solid-state Ti:Al<sub>2</sub>O<sub>3</sub> laser, gain switched by a diode-pumped, Q-switched, frequency-doubled Nd laser, was recently demonstrated by Maker and Ferguson.<sup>1</sup> In this Letter we discuss the development of a low-threshold, cw Ti:Al<sub>2</sub>O<sub>3</sub> laser, including what is to our knowledge the first demonstration of a cw, diode-pumped system. (In this case, diode pumped refers to the indirect process in which a doubled Nd laser acts as an intermediate photon converter.) To our knowledge, the data represent the lowest-threshold Ti:Al<sub>2</sub>O<sub>3</sub> laser reported to date.

Ti:Al<sub>2</sub>O<sub>3</sub> is an unusual laser medium in that the intracavity loss is often dominated by parasitic absorption in the material. This phenomenon has been attributed to the presence of Ti<sup>4+</sup> ions in the crystal (the active ion is Ti<sup>3+</sup>), and it can be tempered by annealing.<sup>2</sup> The crystal quality is characterized in terms of an absorption figure of merit (FOM) defined as the ratio of the peak absorption at 490 nm to the parasitic absorption at 800 nm (the latter is weakly dependent on wavelength in the fluorescence region). Material with a FOM > 100 (for π-polarized light) is commercially available, although the FOM generally decreases as the Ti concentration (i.e., the peak absorption) increases. This is a particularly critical design issue for the case of the low-threshold Ti:Al<sub>2</sub>O<sub>3</sub> laser, where it is necessary to trade off pump-absorption efficiency against intracavity loss.

Laser performance can be analyzed by using a two-dimensional model for a longitudinally pumped system in which both lasers are assumed to operate in a fundamental Gaussian mode.<sup>3</sup> The cw threshold power  $P_{TH}$ , measured at the output of the pump laser, is given by the following equation:

$$P_{TH} = \eta_c \frac{\pi h \nu_p}{4\sigma\tau} (T + L_{CAV} + L_{XTL})(w_0^2 + w_p^2) \times [1 - \exp(-\alpha l)]^{-1}, \quad (1)$$

where  $\eta_c$  is the coupling efficiency between the pump laser and the laser crystal,  $h\nu_p$  is the pump photon energy,  $\sigma$  is the emission cross section,  $\tau$  is the upper-state lifetime, and the final term in brackets represents the pump-absorption efficiency ( $\alpha$  is the absorption coefficient at  $\nu_p$  and  $l$  is the crystal length). The cavity-mode and pump radii in the crystal are given by  $w_0$  and  $w_p$ , respectively. The round-trip cavity losses consist of  $T$  (transmission losses),  $L_{CAV}$  (intracavity losses exclusive of parasitic absorption in the crystal), and  $L_{XTL}$  (parasitic absorption), as given by

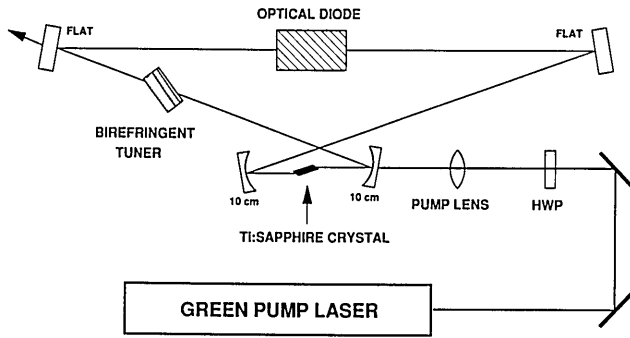
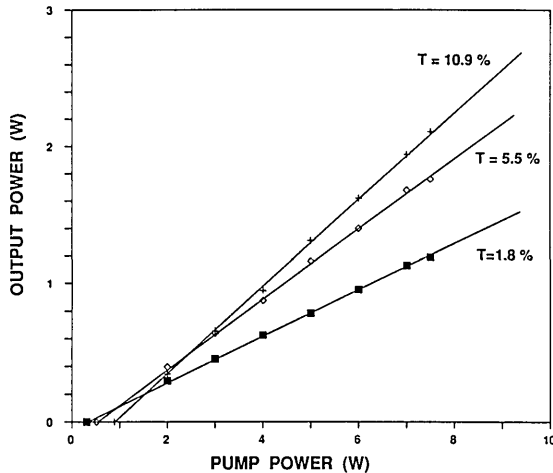
$$L_{XTL} = [1 - \exp(-\alpha l_{eff}/FOM)], \quad (2)$$

where  $l_{eff}$  is the effective parasitic absorption length, as discussed below. The relation for the laser slope efficiency  $\eta_s$  is

$$\eta_s = f_{ovl} \eta_c \left( \frac{\nu_0}{\nu_p} \right) \left( \frac{T}{T + L_{CAV} + L_{XTL}} \right) \times [1 - \exp(-\alpha l)], \quad (3)$$

where  $f_{ovl}$  is an overlap parameter representing the fraction of the absorbed pump power that falls within the cavity mode volume, and the first term within parentheses is the quantum defect. An examination of Eqs. (1)–(3) underscores the basic low-threshold design philosophy: use a short, heavily doped Ti:Al<sub>2</sub>O<sub>3</sub> crystal in a resonator with a small waist in the crystal. The designs that follow were the result of iterative analyses based on a range of available material (as characterized by  $\alpha$  and FOM).

Figure 1 is a schematic of the Ti:Al<sub>2</sub>O<sub>3</sub> ring laser. The four-mirror, figure-eight cavity includes a Brewster-cut gain element, a multiplate birefringent filter for broad tuning, and an optical diode to ensure unidirectional oscillation. Alternatively, the laser can be operated in a standing-wave (sw) configuration by repositioning the flat mirrors for retroreflection, thereby eliminating the path through the optical diode. The fold angle common to the two crossing legs of the

Fig. 1. Schematic of the cw Ti:Al<sub>2</sub>O<sub>3</sub> laser.Fig. 2. Input-output data for the sw laser ( $l = 7.6$  mm) obtained with three output couplers ( $T = 1.8\%$ ,  $5.5\%$ , and  $10.9\%$ ).

resonator is designed for astigmatic compensation. The laser is longitudinally pumped by a cw, green laser that is linearly polarized in the plane of the cavity. Ti:Al<sub>2</sub>O<sub>3</sub> has a broad absorption feature that permits efficient pumping over the range of  $\sim 480$ – $550$  nm [the absorption coefficient at 532 nm is  $\sim 75\%$  of that at the peak near 500 nm (Ref. 4)]. A half-wave plate (HWP) is used to achieve the desired orientation of the pump polarization.

A Brewster-cut crystal is used primarily to avoid limitations associated with the coatings required for normal-incidence operation. Additional benefits include enhanced polarization selectivity and facilitation of a nonastigmatic, compact resonator. However, the laser threshold is higher than it would be in a comparable resonator with a normal-incidence crystal owing to the refraction at the crystal surfaces. The difference is specifically accounted for in the case of a Brewster-cut crystal by multiplying  $P_{TH}$  as expressed in Eq. (1) by the index of refraction  $n$  of the crystal.

A laser of the type shown in Fig. 1 was constructed with 10-cm radius-of-curvature mirrors surrounding a 7.6-mm crystal. The crystal length was chosen to match the confocal parameter of the cavity. Taking advantage of the wavelength dependence of the confocal parameter, we chose the pump lens to match the cavity mode at the crystal facets while underfilling the

mode within the crystal. Input-output characteristics at 800 nm are shown in Fig. 2.<sup>5</sup> The data were obtained with a sw cavity by use of three output couplers (with transmissions  $T = 1.8\%$ ,  $5.5\%$ , and  $10.9\%$ ) and with an Ar-ion pump laser operating on all lines. The input power refers to the power incident upon the HWP. These data are in good agreement with those of the two-dimensional model (Table 1). In this case,  $l_{eff} = 2l$  was used in Eq. (2) to account for the fact that a single round trip corresponds to two passes through the Ti:Al<sub>2</sub>O<sub>3</sub> crystal. Figure 2 demonstrates the trade-off that can be made between threshold and slope efficiency in order to meet the constraints imposed by the pump laser and the experimental power requirements.

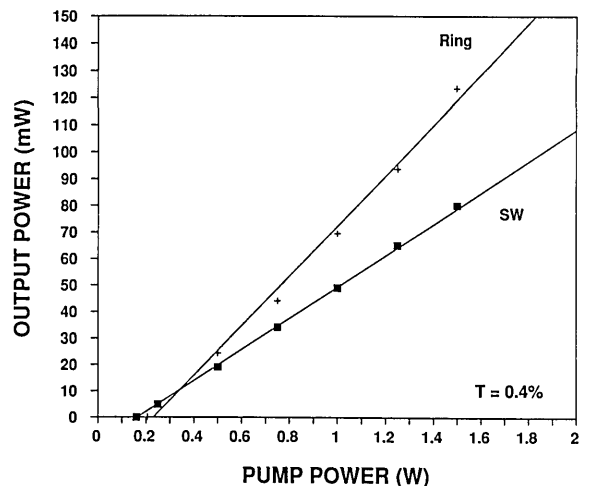
In a ring cavity,  $l_{eff} = l$  so that the parasitic absorption is reduced by a factor of 2 when the sw resonator is converted to a ring. This often leads to enhanced performance, depending on the insertion loss associated with the optical diode. Figure 3 shows input-output data obtained at 800 nm with the same laser as for the previous data but with an output coupler with very low transmission ( $T = 0.4\%$ ).<sup>5</sup> Data are shown for the laser in both the sw and ring configurations.

If we assume reasonable pump overlap, Eq. (1) indicates that the threshold power of a longitudinally pumped laser is roughly proportional to the area of the cavity mode in the crystal. Calculations based on the familiar ABCD matrix formalism for Gaussian beams determined that with the 10-cm mirrors, the minimum

Table 1. Comparison of Measured and Calculated Performance of Standing-Wave Laser at 800 nm<sup>a</sup>

$T$ (%)	Measured		Calculated	
	$P_{TH}$ (W)	$\eta_s$ (%)	$P_{TH}$ (W)	$\eta_s$ (%)
10.9	0.89	32	0.74	36
5.5	0.52	26	0.49	27
1.8	0.31	17	0.33	13
0.4	0.15	6	0.26	4

<sup>a</sup> The parameters are  $\eta_c = 0.95$ ,  $\sigma = 3.5 \times 10^{-19}$  cm<sup>2</sup>,  $\tau = 3.2$   $\mu$ s,  $L_{CAV} = 0.01$ ,  $w_0 = 25$   $\mu$ m,  $w_p = 12.5$   $\mu$ m,  $\alpha = 2.96$  cm<sup>-1</sup>,  $l = 7.6$  mm, FOM = 100,  $f_{ovl} = 1$ , and  $n = 1.75$ .

Fig. 3. Input-output data for the sw and ring lasers ( $l = 7.6$  mm) with a low-threshold output coupler ( $T = 0.4\%$ ).

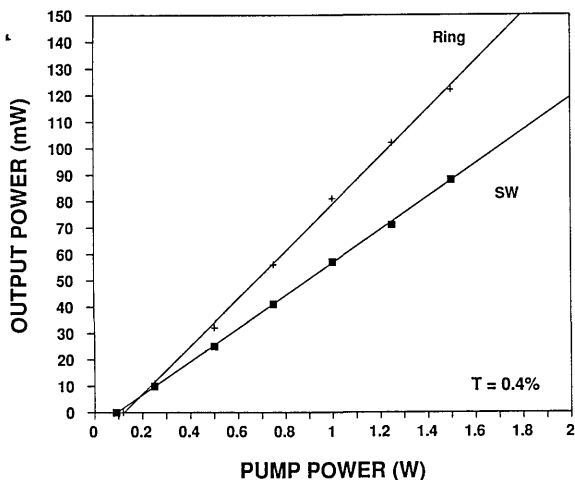


Fig. 4. Input-output data for the sw and ring lasers ( $l = 3.5$  mm) with a low-threshold output coupler ( $T = 0.4\%$ ).

radius of the  $TEM_{00}$  mode in the crystal is  $\sim 25 \mu\text{m}$ . With 5-cm mirrors, this is reduced to  $\sim 16 \mu\text{m}$ .

A second laser was constructed with 5-cm mirrors and a 3.5-mm  $Ti:Al_2O_3$  crystal. The crystal was fabricated from the same boule as the 7.6-mm crystal. Figure 4 shows a comparison of the performance of the laser operating at 800 nm with the  $T = 0.4\%$  output coupler in the sw and ring configurations. The threshold power in the sw configuration, measured at the input to the HWP, was 90 mW. The output power was 57 mW at a pump power of 1 W. The threshold for the unidirectional, single-frequency, ring laser was 119 mW, with 81 mW of power obtained at a pump power of 1 W. The data of Fig. 3 were obtained with the Ar-ion laser operating at 514.5 nm. The measured absorption coefficient of the  $Ti:Al_2O_3$  crystal at that wavelength was  $2.84 \text{ cm}^{-1}$ .

The performance obtained with the 5-cm mirrors was adequate to demonstrate diode-pumped operation in both the sw and ring configurations with a commercially available diode-pumped, doubled, Nd:YAG laser (Adlas model DPY 325C). The device emitted nearly 175 mW of power at 532 nm in a linearly polarized, near-diffraction-limited beam. In the sw configuration, the measured threshold power was 97 mW at 800 nm, with 59% of the pump light absorbed in

the crystal. The output power at 800 nm was 4.2 mW, with 173 mW of power input to the pump lens, and the laser was tunable from 771 to 844 nm. In an effort to use the pump more efficiently, the pump beam transmitted by the crystal was retroreflected and reimaged. With pumping in this way from both directions, the output power of the  $Ti:Al_2O_3$  laser was 6.0 mW, although the power stability was poor owing to feedback to the pump laser. In principle, this problem could be alleviated with adequate isolation. The measured threshold in the ring configuration at 800 nm was 120 mW, and 3.1 mW of power was obtained at an input power of 173 mW. The ring laser was tunable from 775 to 829 nm. Single-frequency operation was verified with a scanning Fabry-Perot interferometer.

While the maximum power was clearly limited, it is interesting to note that the performance obtained with the diode-pumped green source was comparable with that obtained with the Ar-ion laser. Under operation at 800 nm, the smaller quantum defect partially offsets the lower absorption cross section. However, the results are a strong indication that the beam quality of the diode-pumped green laser is at least as good as that of the Ar-ion laser used here.

In summary, a cw, single-frequency, diode-pumped  $Ti:Al_2O_3$  laser has been demonstrated. A source of this type may lead to practical applications in areas such as remote sensing (e.g., as a seed source for a pulsed, high-energy system) and spectroscopy. These will expand as available diode-pumped green lasers increase in power and become more affordable.

The authors acknowledge the support and generosity of Gerhard Marcinkowski and thank Adlas for their loan of equipment. This research was supported in part by the NASA Langley Research Center.

## References

1. G. T. Maker and A. I. Ferguson, *Opt. Lett.* **15**, 375 (1990).
2. M. Kokta, U.S. patent 4,836,953.
3. P. F. Moulton, *IEEE J. Quantum Electron.* **QE-21**, 1582 (1985).
4. P. F. Moulton, *J. Opt. Soc. Am. B* **3**, 125 (1986).
5. J. Harrison, G. A. Rines, and P. F. Moulton, in *Conference on Lasers and Electro-Optics*, Vol. 11 of 1989 OSA Technical Digest Series (Optical Society of America, Washington, D.C., 1989), paper MC1.